In search of early life: Carbonate veins in Archean metamorphic rocks as potential hosts of biomarkers

Carl A. Peters[1,*], Sandra Piazolo[1], Gregory E. Webb[2], Adriana Dutkiewicz[3], Simon C. George[1]

[1]Department of Earth and Planetary Sciences, Macquarie University, North Ryde, NSW 2109, Australia

[2]School of Earth Sciences, The University of Queensland, St. Lucia, QLD 4072, Australia

[3]EarthByte Group, School of Geosciences, University of Sydney, NSW 2006, Australia

**Corresponding author. Email: carl.peters@mq.edu.au*

ABSTRACT

The detection of early life signatures using hydrocarbon biomarkers in Precambrian rocks struggles with contamination issues, unspecific biomarkers and the lack of suitable sedimentary rocks due to extensive thermal overprints. Importantly, host rocks must not have been exposed to temperatures above 250°C as at these temperatures biomarkers are destroyed. Here we show that Archean sedimentary rocks from the Jeerinah Formation (2.63 billion years) and Carawine Dolomite (2.55 billion years) of the Pilbara Craton (Western Australia) drilled by the Agouron Institute in 2012, which previously were suggested to be suitable for biomarker studies, were metamorphosed to the greenschist facies. This is higher than previously reported. Both the mineral assemblages (carbonate, quartz, Fe-chlorite, muscovite, microcline, rutile, and pyrite with absence of illite) and chlorite geothermometry suggest that the rocks were exposed to temperatures higher than 300°C and probably ~ 400°C, consistent with greenschist-facies metamorphism. This facies leads to the destruction of any biomarkers and explains why the extraction of hydrocarbon biomarkers from pristine drill cores has not been successful. However, we show that the rocks are

cut by younger formation-specific carbonate veins containing primary oil-bearing fluid inclusions and solid bitumens. Type 1 veins in the Carawine Dolomite consist of dolomite, quartz and solid bitumen, whereas type 2 veins in the Jeerinah Formation consist of calcite. Within the veins fluid inclusion homogenisation temperatures and calcite twinning geothermometry indicate maximum temperatures of ~ 200°C for type 1 veins and ~ 180°C for type 2 veins. Type 1 veins have typical isotopic values for reprecipitated Archean sea-water carbonates, with $\delta^{13}C_{VPDB}$ ranging from -3‰ to 0‰ and $\delta^{18}O_{VPDB}$ ranging from -13‰ to -7‰, while type 2 veins have isotopic values that are similar to hydrothermal carbonates, with $\delta^{13}C_{VPDB}$ ranging from -18‰ to -4‰ and $\delta^{18}O_{VPDB}$ ranging from -18‰ to -12‰. Evidently, the migration and entrapment of hydrocarbons occurred after peak metamorphism under temperatures congruous with late catagenesis and from fluids of different compositions. The relatively high temperatures of vein formation and the known geotectonic history of the rocks analysed suggest a probable minimum age of 1.8 billion years (Paleoproterozoic). Our results demonstrate that post peak-metamorphic veins provide an exciting opportunity in the search for evidence of early life. The integration of petrological and organic geochemical techniques is crucial for any future studies that use biomarkers to reconstruct the early biosphere.

Keywords: Early Life, Archean, Pilbara Craton, Organic Matter, Carbonate Veins, Biomarkers

1. INTRODUCTION

The search for evidence of life in the Archean eon (> 2.5 billion years), its composition and impact on Earth's environment relies on the occurrence of microfossils, stromatolites, and on the analysis of stable isotopes and hydrocarbon biomarkers (Dutkiewicz et al., 2006; Waldbauer et al., 2009; Kamber et al., 2014; Planavsky et al., 2014; Brasier et al., 2015; Stüeken et al., 2015). Biomarkers are organic compounds that have particular biosynthetic origins and are preserved as part of the organic matter of sediments and sedimentary rocks (Peters et al., 2005; Killops and Killops, 2009) and can be used as a source of information, especially where microfossils are absent. However, the field of Archean biomarker research has recently encountered major pitfalls. In a recent study to reappraise biomarkers believed to be indigenous to Archean sedimentary rocks from the Pilbara Craton (Western Australia; Brocks et al., 1999; 2003; Eigenbrode et al., 2008), French et al. (2015) demonstrated that previously detected steranes and hopanes indicative for eukaryotes and bacteria were, in fact, the result of sample contamination. This had been suggested by an earlier study of the carbon isotopic composition of the kerogen and extracted hydrocarbons (Rasmussen et al., 2008). These biomarkers previously were considered to support the presence of oxygenic photosynthesis prior to the Great Oxidation Event (GOE) ca. 2.45 billion years (Ga) ago, and coincided well with inorganic evidence for "whiffs" of oxygen before oxygen became fully retained in the atmosphere (e.g., Anbar et al., 2007; Planavsky et al., 2014). Consequently, these biomarkers can no longer provide evidence supporting the rise of oxygen-producing bacteria (cyanobacteria) and eukaryotes before the GOE. The rock samples investigated by French et al. (2015) contained ample organic material (up to 6.7% total organic carbon; French et al., 2015), but regional metamorphism was the most likely explanation for the absence of any detectable indigenous biomarkers, with only highly thermally stable hydrocarbons remaining. Indeed,

hydrocarbon biomarkers can be destroyed when exposed to pressures and temperatures consistent with metagenesis (Hunt, 1996). This severely limits the search for Archean biomarkers, since all Pilbara Craton sedimentary rocks from that time were metamorphosed during two major thermo-tectonic events at 2.430–2.40 Ga and 2.215–2.145 Ga (Rasmussen et al., 2005).

A further complication in the reconstruction of the Archean biosphere and environments is the prevalence of "non-specific biomarkers". For example, the most prominent hydrocarbon biomarker for cyanobacteria, 2-methylhopanoid (Summons et al. 1999), has been found in other bacteria strains, and therefore it is not exclusive to cyanobacteria nor suitable for investigating oxygenic photosynthesis (e.g., Rashby et al., 2007; Welander et al., 2010). On the positive side, non-exclusive hydrocarbon biomarkers for cyanobacteria include mid-chain methylheptadecanes (Schirmer et al., 2010), and high abundances of these molecules might still suggest oxygenic photosynthesis. Other biomarkers that would indicate the presence of oxygen include any type of alkylated steranes, which are derived only from eukaryotes and require molecular oxygen for their biosynthesis (Volkman, 2005). Whether eukaryotes were already present in the Archean or evolved later is not known, as the previously detected alkylated steranes in the Pilbara rocks have now been shown to reflect contamination (Rasmussen et al., 2008; French et al., 2015). One of the most persistent complications in the detection of early life using biomarkers is the introduction of hydrocarbons by, for example, more recent oil migration, or during sampling and handling of rock samples, thus requiring careful identification of these contaminants (e.g., Rasmussen et al., 2008; Brocks, 2011).

One way to minimise contamination issues is to analyse oil trapped in fluid inclusions. These oil-bearing fluid inclusions are normally hosted within sealed cavities in mineral grains such as calcite, dolomite, feldspar, and quartz, making them relatively stable when exposed to high temperatures

and pressures (~ 350°C, 2 kbar; e.g., Dutkiewicz et al., 2006; George et al., 2008; 2012). Oil-bearing fluid inclusions have previously been found in a range of Precambrian rocks (Dutkiewicz et al., 1998, 2006; George et al., 2008). They are protected from the degradation processes that can otherwise affect oil in an open pore space, partly because they are closed systems with high fluid pressures, and partly because they contain no clays or other minerals or metals that might catalyse oil-to-gas cracking (George et al., 2008). The included oil thus remains relatively unaltered compared to its host rock, and examples have been successfully analysed in numerous hydrocarbon biomarker studies (e.g., Dutkiewicz et al., 2006; George et al., 2008, 2012). The main problem with the interpretation of oil-bearing fluid inclusion geochemistry is to determine the timing of trapping of hydrocarbon fluids (George et al., 2012).

Nonetheless, the biggest challenge in our view is to find suitable Archean rocks that have experienced adequately low metamorphic grades throughout their geological history such that biomarkers remain intact. Many studies that reported the presence of syngenetic biomarkers in Archean rocks (Brocks et al., 1999; 2003; Eigenbrode et al., 2008; Waldbauer et al., 2009) would have benefited from additional petrological data. As biomarkers can be preserved in different mineral phases or in fractures and cracks (e.g., Nabbefeld et al., 2010, Brocks, 2011) and could therefore represent different origins, it is essential to know the structure of the sample in order to correctly interpret any biomarker data obtained from bulk analysis. With additional petrological data, such as mineral assemblages, an organic geochemist can assess if metamorphosed rocks can still theoretically contain biomarkers before the rocks are analysed for biomarkers using techniques that are relatively expensive and time-consuming. With this supporting information it may be much easier to assess any potential contamination problems and to provide independent constraints on the relative timing of oil generation and migration. For example, one would not expect

biomarkers to persist in rocks that have been heated to temperatures in excess of ~ 250ºC (e.g., Hunt, 1996).

In this study, we document the presence of oil-bearing fluid inclusions and solid bitumens in carbonate veins of new ultra-clean drilled Archean rock samples from the Pilbara Craton. Our approach includes an extensive petrological characterisation of sedimentary host rocks, veins and oil-bearing fluid inclusions that reveal different grades of metamorphism between the host rock and the veins, making the oil-bearing fluid inclusions and solid bitumens promising targets for biomarker analyses.

1.1 Geological setting

The Agouron Institute Drilling Program (AIDP) drilled three ca. 300 m-long cores in the Pilbara Craton in 2012 (Fig. 1; French et al., 2015), in order to obtain fresh, unadulterated Archean rocks for helping to unravel early life signatures during the Archean using hydrocarbon biomarkers, light stable isotopes, transition metal isotopes, and redox-sensitive detrital minerals.

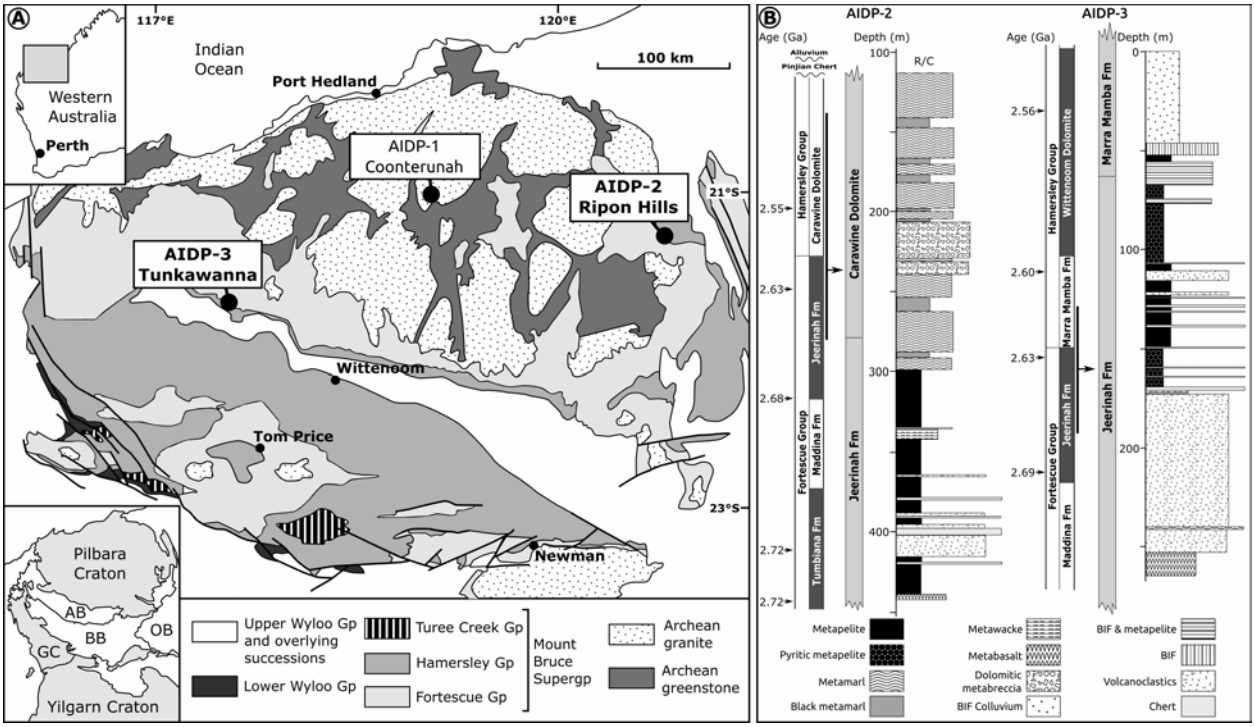

Figure 1: (A) Regional map showing the geology of the Pilbara Craton, Western Australia, and the locations of the Agouron Institute Drilling Program (AIDP) drill sites (AIDP-1: 21°06'38"S, 119°06'4"E; AIDP-2: 21°16'51"S, 120°50'2"E; AIDP-3: 21°46'32"S, 117°34'11"E. AB - Ashburton Basin; BB - Bangemall Basin; OB - Officer Basin; GC - Gascoyne Complex. (B) Lithologies of the AIDP-2 and AIDP-3 drill cores. Modified after Rasmussen et al. (2005) and French et al. (2015).

Core AIDP-1 was drilled in the Coonterunnah Subgroup of the Warrawoona Group, Pilbara Supergroup (21°06'38"S, 119°06'4"E), and includes the metamorphosed volcanic Coucal Formation (3.52 Ga; Van Kranendonk et al., 2007). As this core was drilled as a negative control sample for biomarkers and does not contain oil-bearing fluid inclusions it will not be discussed further (see S-Fig. 1 for a detailed AIDP-1 sample description). Core AIDP-2 was drilled in the

137 Ripon Hills region (21°16'51"S, 120°50'2"E) and core AIDP-3 was drilled in the Tunkawanna
138 region (21°46'32"S, 117°34'11"E; Fig. 1A,B). Core AIDP-2 represents a relatively shallow water
139 facies and includes the Carawine Dolomite (2.55–2.54 Ga) of the Hamersley Group that
140 conformably overlies the Jeerinah Formation (2.69–2.63 Ga) of the Fortescue Group. AIDP-3 is a
141 time-equivalent core in a deeper water facies compared to AIDP-2, and includes the Marra Mamba
142 Iron Formation (~ 2.60 Ga) of the Hamersley Group, conformably overlying the Jeerinah
143 Formation (French et al., 2015). Both cores were drilled in areas where syngenetic biomarkers of
144 Archean age were reported at the same stratigraphic levels (e.g., Brocks et al., 1999; Eigenbrode
145 et al., 2008), and where the metamorphic facies was perceived to be adequately low grade for
146 biomarkers to be preserved (prehnite-pumpellyite facies: < 300°C, < 7 kbar; e.g., Smith et al.,
147 1982; French et al., 2015). The Carawine Dolomite and Jeerinah Formation are the primary targets
148 of this study as they appear to contain suitable host lithologies in which oil-bearing fluid inclusions
149 can be found. The Jeerinah Formation comprises shale, chert, siltstone, and minor sandstone,
150 dolomite, conglomerate and localised fault breccias (Thorne and Trendall, 2001). During
151 deposition of the Jeerinah succession there was a marked regional change from volcanism and
152 shallow-water sedimentary deposition to deeper water deposition, indicating a northerly marine
153 transgression in a deepening basin (Thorne and Trendall, 2001). The Carawine Dolomite appears
154 to be the lateral time-equivalent of banded iron formations that include the Marra Mamba Iron
155 Formation and interbedded carbonate units such as the Wittenoom Dolomite to the west and
156 southwest of the Pilbara Craton (Simonson and Hassler, 1997; Fig. 1A). The Carawine Dolomite
157 is a well-bedded, stromatolitic to massive carbonate unit with interbedded chert near the base.
158 Simonson et al. (1993) interpreted the Carawine Dolomite predominantly as a carbonate platform
159 deposit formed in a shallow water environment (< 100 m), based on the presence of abundant

160 stromatolites, oncoids, ripple marks and local evaporites, but noted that a deeper water dolomite
161 facies occurs as well.

162 In general, the Hamersley and Fortescue groups have experienced low-grade metamorphism
163 (lower prehnite-pumpellyite facies to lower greenschist facies) due to burial beneath > 5 km of the
164 2.45–2.41 Ga Turee Creek Group (Smith et al., 1982), before the initial folding, uplift and partial
165 erosion of the complete 2.78–2.43 Ga Mount Bruce Supergroup, which includes the Fortescue,
166 Hamersley, and Turee Creek groups. The last uplift of the Mount Bruce Supergroup is recorded in
167 the 2.0 Ga lower Wyloo Group, which experienced further deformation, uplift and erosion, and
168 deposition of part of the 1.8 Ga upper Wyloo Group (e.g., Schmidt and Clark, 1994). Regional-
169 scale fluid flow occurred during the 2.43–2.40 Ga and 2.215–2.145 Ga metamorphic and
170 deformational events (Rasmussen et al., 2005).

171 **2. MATERIALS & METHODS**

172 **2.1 Sample preparation**

173 A total of 88 samples from different lithologies including the Jeerinah Formation and Carawine
174 Dolomite were sampled in July 2013 and March 2014 from three AIDP drill cores stored at the
175 Geological Survey of Western Australia: 11 samples were taken from AIDP-1, 54 from AIDP-2,
176 and 23 from AIDP-3 (see supplementary information S-Table 1 for detailed sample descriptions
177 and methods used). The sample set that was investigated for biomarkers by French et al. (2015)
178 covers the same formations and drill cores. Doubly-polished 100–120 μm sections were prepared
179 from 51 samples that were considered potential host rocks for oil-bearing fluid inclusions. The
180 polished sections were analysed using optical and UV microscopy for microstructural
181 characterisation and fluid inclusion analyses, scanning electron microscopy (SEM) for

microstructural characterisation and mineral identification, and laser ablation inductively coupled plasma-mass spectrometry (LAM-ICP-MS) for potential radiometric dating and rare earth element analysis. Polished blocks from four samples that lack polished sections were also assessed using SEM. Prior to SEM analysis, the polished sections and polished blocks were carbon coated.

Twenty-one samples were prepared as < 120 μm fine rock powder for stable isotope analysis. Veins were cut out of the rock matrix using a Buehler IsoMet® 4000 linear precision saw. Two samples that have dolomite inter-grown in narrow calcite veins were disaggregated using a Siemens selFrag® high-voltage electric pulse disintegrator. The particles were then separated using a Frantz® LB-1 magnetic barrier separator. The following voltages were used to separate matrices from vein calcite: 106 kV to collect calcite, followed by 40-106 kV to collect matrix dolomite. The separation of veins by both the precision saw and the disintegrator resulted in 30 fractions of dolomite or calcite, which were hand-crushed and pulverised ready for stable isotope analysis.

2.2 Microstructure and Fluid Inclusion Petrography

Images of microstructures under plane polarised and crossed polarised light were taken with a Nikon Eclipse 50i POL optical microscope equipped with a Nikon DS-Fi1 digital camera. Selected samples (both polished sections and blocks) were investigated using a Zeiss EVO MA15 Scanning Electron Microscope to obtain electron backscatter images revealing microstructural features.

All polished sections were examined under an Olympus BX63 optical microscope with an ultraviolet (UV) attachment using a medium-width bandpass excitation filter (330-385 nm) and a longpass barrier filter (420 nm). Oil-bearing fluid inclusions were recognised by their fluorescence under UV excitation, which is caused by aromatic hydrocarbons and some polar compounds (e.g., George et al, 2001).

Homogenisation and ice-melting temperatures of fluid inclusions (Goldstein and Reynolds, 1994) were measured using a Linkam THMS 600 heating–freezing stage attached to an Olympus BX60 optical microscope. The stage was calibrated using synthetic H_2O and CO_2 fluid inclusions with precision of ± 0.2°C for ice-melting temperatures and ± 2°C for homogenising temperatures. The majority of oil-bearing fluid inclusions leaked during analysis and were disregarded from further analysis. Primary aqueous fluid inclusions from growth bands in large carbonate crystals of carbonate veins were used to measure homogenisation and ice melting temperatures.

2.3 Major, Minor, and Trace Elemental Analysis

A detailed mineralogical investigation was performed using the Zeiss EVO MA15 SEM with Oxford Instruments Aztec® Synergy Energy-Dispersive X-ray Spectroscopy (EDS). For EDS spot analysis the beam was operated at 15 kV accelerating voltage and 20 nA beam current, with an acquisition time of 60 s and a working distance of ~ 12 mm. Backscattered electron (BSE) images were taken in conjunction with spot analyses. Data collection and processing was conducted using Oxford Aztec® software.

Trace element concentrations (including rare earth elements (REE), Y, Ba, Rb, Sr, Th, U, Nb, Ta, Pb, Zr, Hf, Y, Sc, V, Co, Zn, and Cr) were determined for polished sections using a Photon Machines Excite Excimer laser ablation system attached to an Agilent 7700X ICP-MS. ICP-MS operating conditions were set to 1400 W forward power and gas flows as follows: carrier 1 L(Ar)/min, sample chamber 0.8 L(He)/min. The counting time for one analysis was typically 180 s (60 s on gas blank to establish background and 120 s for signal collection). Laser beam conditions were set as follows: diameter of the laser beam was around 50 µm, the frequency was 5 Hz, and the power source was 6 J/cm^2. Data were processed using the GLITTER® software. The NIST-610

standard was used to calibrate the relative element sensitivities for the trace element analyses. Each analysis was normalised to Ca using concentrations determined by SEM. Detection limits for each element were usually in the range 0.01–0.06 ppm. The average precision (1σ standard deviation) for all elements was 0.32%. This estimation is based on the results for the BCR-2 standard that was run twice in the beginning and twice at the end of each run.

2.4 Geothermometers

Mineral assemblages to assess the metamorphic facies of the sedimentary rocks and chlorite geothermometry as described by Lanari et al. (2014) are based on the chemical data obtained by SEM-EDS as described above. Because the SEM-EDS data does not provide $(Fe^{3+}/\Sigma Fe)_{Chl}$ values, in order to calculate chlorite geothermometer "Chl(1)" all iron in the chlorites was assumed to be in the ferrous state ($\Sigma Fe = Fe^{2+}$) for the calculation of chlorite geothermometer "Chl(2)". Calcite deformation twin widths and intensities are correlated to changes in temperature (Passchier and Trouw, 2005). The widths and frequencies of calcite twins were measured as described by Ferrill et al. (2004) using captured images, so as to determine deformation temperatures. All assessed calcite twins were tapered towards the grain boundaries and therefore confirmed as deformation twins, which is important for the validity of calculated temperatures. In comparison, growth twins are commonly straight and stepped (Passchier and Trouw, 2005). In addition to the calcite geothermometer, homogenisation temperatures of fluid inclusions were assessed as described above, as these temperatures estimate the minimum temperatures at which fluid inclusions were trapped inside the mineral grain (Goldstein and Reynolds, 1994).

2.5 Stable isotopes

Carbon and oxygen stable isotope compositions were analysed for 30 calcite, dolomite, and ankerite samples. Fifteen samples were veins and fifteen were from the host rocks. The estimated carbonate content varied between 5 and 100%, but only three of the rock matrix samples from the Jeerinah Formation contained less than 70% carbonate. The measurements were made using a Finnigan MAT 251 Isotope-Ratio Mass Spectrometer (IRMS) with a Kiel IV carbonate device. Samples were reacted with 4 drops of 106% phosphoric acid at 75°C for 16 min with live trapping of evolved gases. The NBS-18 standard was analysed at the beginning of the sequence, and the NBS-19 standard was analysed stepwise during the sequence. Isotopic compositions of oxygen and carbon were normalised to the NBS-19 standard having $\delta^{18}O_{VPDB}$ = -1.41‰ and $\delta^{13}C_{VPDB}$ = -1.95‰. The external precisions (1σ standard deviation) for isotopic analyses were typically as follows: $\delta^{18}O_{VPDB} \leq 0.06$‰ and $\delta^{13}C_{VPDB} \leq 0.03$‰ for calcite, and $\delta^{18}O_{VPDB} \leq 0.1$‰ and $\delta^{13}C_{VPDB} \leq 0.03$‰ for dolomite/ankerite. These estimates are based on the results for the concurrently run NBS-19 and NBS-18 standards.

3. RESULTS & DISCUSSION

3.1 Assessment of the metamorphic facies

The Carawine Dolomite in AIDP-2 core consists mainly of fine-grained and laminated facies with minor coarser facies that include breccia, pressure-solution surfaces, and stromatolites. All facies have abundant stylolites, which are sub-parallel to bedding. The major mineral assemblage in the Carawine Dolomite includes dolomite (Fig. 2), quartz, chlorite (brunsvigite, chamosite, diabantite; S-Fig. 1), muscovite, microcline, rutile and pyrite (Table 1, Fig. 3A). The Jeerinah Formation in AIDP-2 and AIDP-3 drill cores consists mainly of plane-laminated black shale. Layers, nodules, and lenses of disseminated pyrite are included in the shales and are more abundant in AIDP-2. The

major mineral assemblage in the Jeerinah Formation includes carbonate (dolomite, calcite, and siderite/rhodochrosite; Fig. 2), quartz, chlorite (brunsvigite, chamosite, diabantite, thuringite; S-Fig. 1), muscovite, albite, microcline, rutile, stilpnomelane and pyrite (Table 1, Fig. 3B). These mineral assemblages in all the investigated samples of the AIDP-2 and AIDP-3 cores indicate greenschist-facies metamorphism (Bucher and Grapes, 2011). In addition, both formations are devoid of illite, which is another important indicator for the onset of greenschist-facies metamorphism, because illite transforms into muscovite, which is present in the mineral assemblages, during recrystallisation (e.g., Gharrabi et al., 1998). In general, the carbonate-rich sediments (mainly from the Carawine Dolomite) and the shales (mainly from the Jeerinah Formation) have been transformed into metamarls and metapelites, respectively.

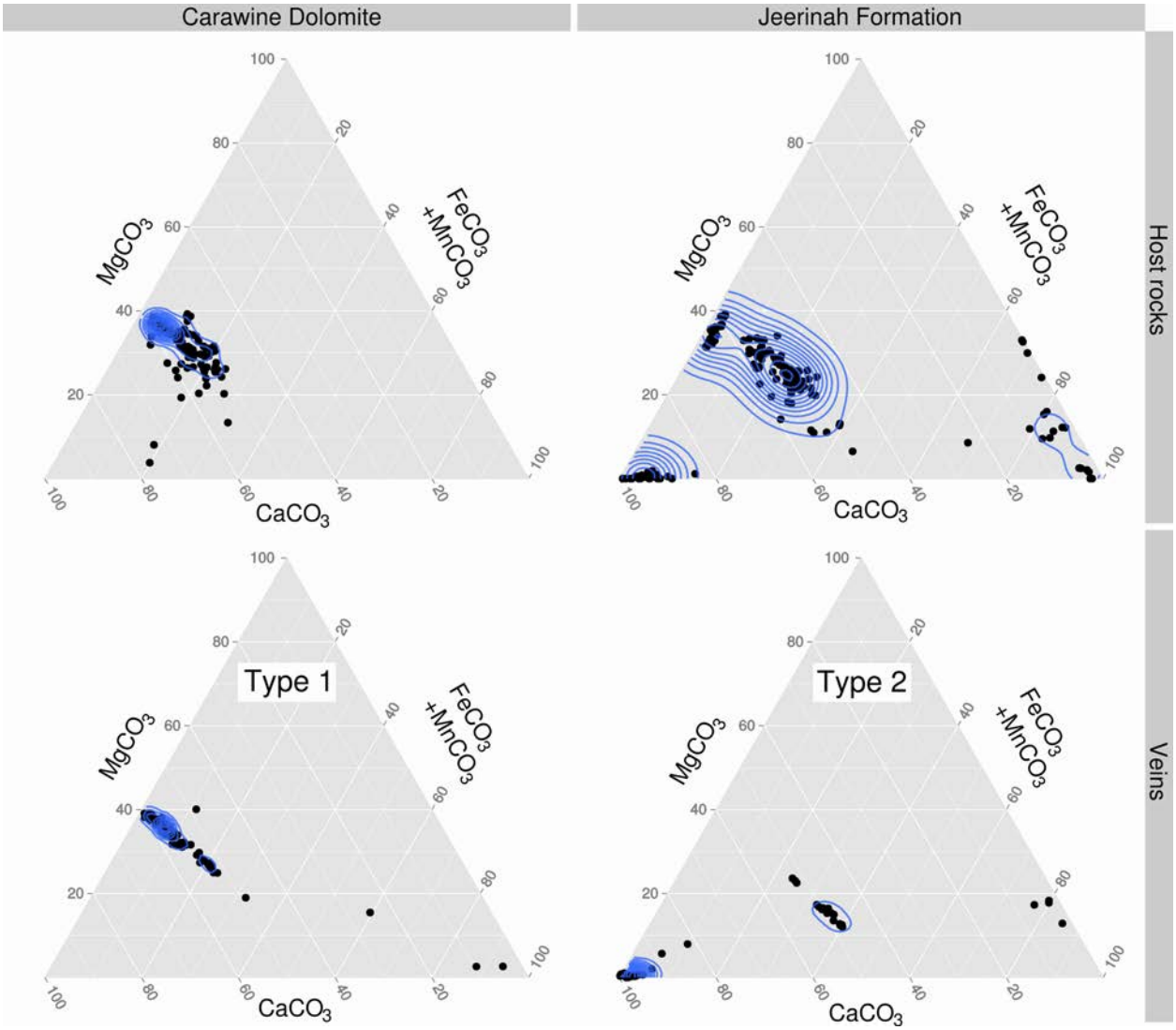

280

281 **Figure 2:** Carbonate compositions for the Carawine Dolomite and the Jeerinah Formation,
282 distinguishing host rocks (upper panels) and veins (lower panels). Type 1 veins refer to a dolomitic
283 composition, similar to their host rock, and type 2 veins refer to a calcite composition. Filled black
284 circles represent SEM/EDS data based on 584 spot analyses on single carbonate minerals of 19
285 samples from AIDP-2 and AIDP-3 cores. Density lines represent the bivariate normal distribution.
286 $MgCO_3$ = magnesite; $CaCO_3$ = calcite; $FeCO_3$ = siderite; $MnCO_3$ = rhodochrosite.

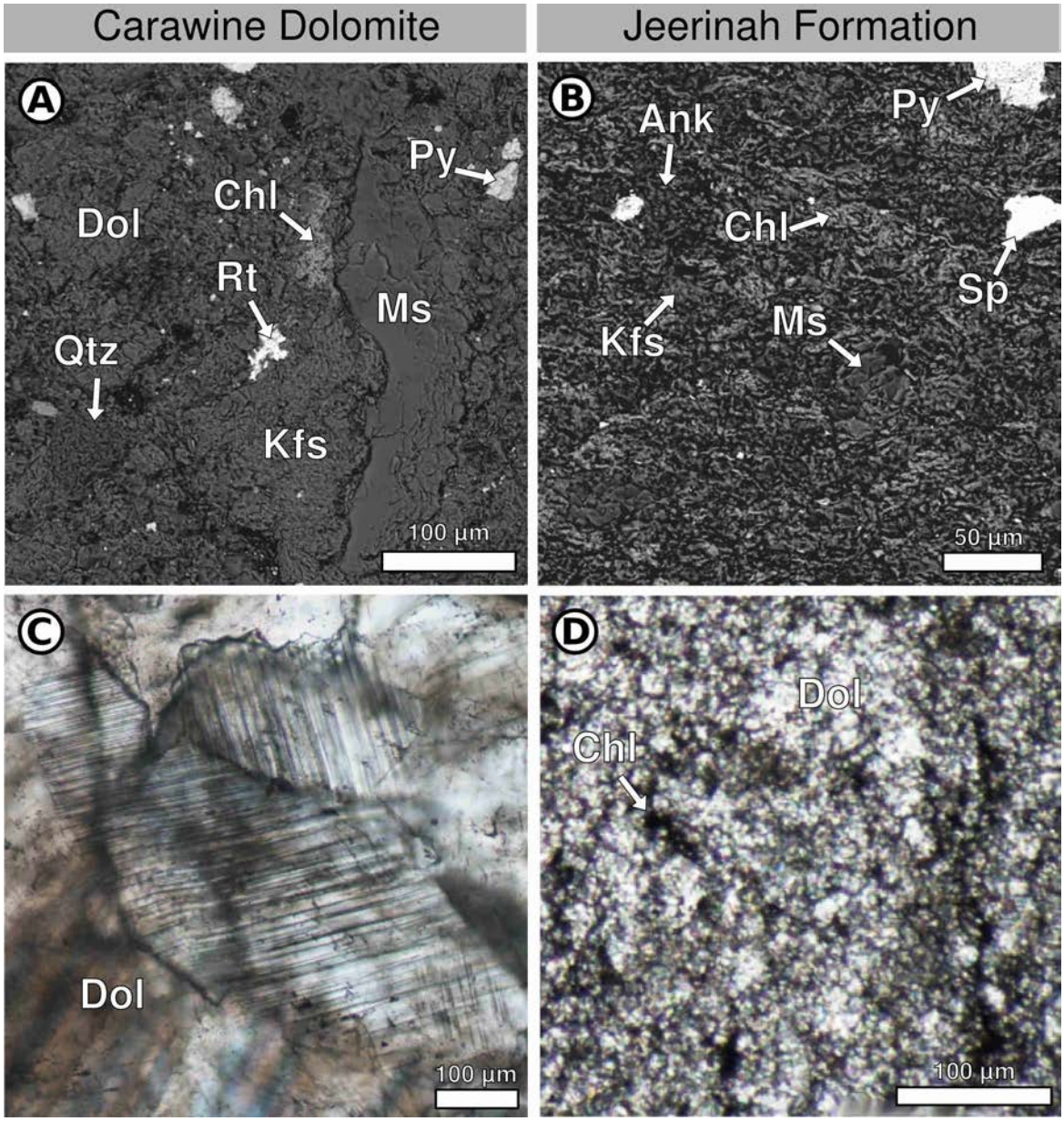

287

288 **Figure 3:** Mineralogy and microstructures of AIDP sedimentary rocks. (A,B) SEM backscatter
289 images showing the mineral assemblages and (C,D) photomicrographs of the microstructures
290 under plane polarisation. (A) Black dolomitic metamarl of the Carawine Dolomite (AIDP-2/258.69
291 m, S30). (B) Black metapelite of the Jeerinah Formation (AIPD-3/118.62 m, S67). (C) Subhedral
292 dolomites with deformation twins and deformation lamellae between anhedral dolomites (AIDP-
293 2/209.79 m, S23; Carawine Dolomite). (D) Anhedral dolomite matrix with chlorites (AIDP-

2/292.41 m, S36; Jeerinah Formation). Dol = dolomite, Chl = chlorite, Py = pyrite, Qtz = quartz, Rt = rutile, Ms = muscovite, Kfs = K-feldspar, Ank = ankerite, Sp = sphalerite.

Table 1: Major mineral assemblages and chlorite geothermometry from sedimentary rocks of AIDP-2 and AIDP-3 boreholes.

Sample	Mineral assemblage	$T_{Chl(2)^{2kbar}}$ [°C]	$T_{Chl(2)^{2.5kbar}}$ [°C]	$Tchl2_{Chl(2)^{3kbar}}$ [°C]	n
AIDP-2/149.39m (S11)	Chl+Qtz+Cb+Ms+Kfs+Rt+Py	403±107	411±108	419±109	14
AIDP-2/258.66m (S30)	Chl+Qtz+Cb+Ms+Kfs+Rt+Py	498±106	507±107	516±108	3
AIDP-2/330.63m (S45)	Chl+Qtz+Cb+Ms+Ab+Rt+Py	412±41	420±42	428±42	25
AIDP-2/337.94m (S48)	Chl+Qtz+Cb+Ms+Ab+Rt+Py	415±66	423±67	431±68	22
AIDP-2/364.67m (S52)	Chl+Qtz+Cb+Ms+Rt+Py	344±77	352±78	359±79	4
AIDP-2/419.40m (S56)	Chl+Qtz+Cb+Stp+Py	309±36	315±36	323±37	11
AIDP-3/72.11m (S61)	Chl+Qtz+Cb+Ms+Kfs+Rt+Py	417±83	425±84	433±85	10
AIDP-3/118.56m (S67)	Chl+Qtz+Cb+Ms+Kfs+Ab+Rt+Py	354±119	361±121	369±122	27
AIDP-3/162.65m (S77)	Chl+Qtz+Cb+Ms+Kfs+Rt+Py	497±81	506±82	515±83	11

Microstructures suggest the occurrence of extensive grain boundary area reduction in all sedimentary carbonates of both the Carawine Dolomite and the Jeerinah Formation (e.g., Fig. 3D). This is a form of recrystallisation that occurs at high temperatures in a monomineralic rock that will reach a state of fabric equilibrium of polygonal crystals (Passchier and Trouw, 2005). Furthermore, twinning of dolomite was detected in subhedral crystals that reflect recrystallised fabrics inside the anhedral dolomite matrix (Fig. 3C). Twinning in dolomite, however, does not occur under 300°C (Passchier and Trouw, 2005), thus providing a minimum temperature limit for the two formations.

Chlorites are Fe-rich and occur in both the AIDP-2 and AIDP-3 cores (S-Fig. 1). Geothermometry based on chlorite [Chl(2), after Lanari et al. (2014)] was carried out for the AIDP-2 and AIDP-3 cores. As mineral assemblages in both cores indicate greenschist facies, and as greenschist-facies metamorphism occurred in the Pilbara Craton at pressures of 2 to 3 kbars for both the Hamersley

312 and Fortescue groups (Smith et al., 1982), three different pressures (2, 2.5 and 3 kbars) were chosen
313 to calculate the temperatures (Table 1). Chlorite geothermometry-based temperatures range from
314 400 to 500°C for the Carawine Dolomite, and 300 to 450°C for the Jeerinah Formation in AIDP-
315 2. For AIDP-3 the temperatures in the Jeerinah Formation are between 350 and 500°C. The Chl(2)
316 thermometer gives relatively large temperature errors of 36–136°C, which may have been due to
317 detrital chlorites given the large variation of chlorite composition (S-Fig. 1). Despite uncertainties
318 regarding the precision of this geothermometer, it is clear that the samples have been exposed to
319 greenschist-facies metamorphism, probably at temperatures of ~ 400°C.

320 Initially, the locations of both AIDP-2 and AIDP-3 were chosen based on the premise that they
321 occur in zones of low regional metamorphism, i.e., prehnite-pumpellyite facies (< 300°C) (Smith
322 et al., 1982; Rasmussen et al., 2005). Indeed, such a relatively low metamorphic grade might allow
323 the preservation of potential syngenetic biomarkers, provided that they survived prolonged burial
324 temperatures well above the oil window (~150°C; Tissot and Welte, 1984). The metamorphic
325 facies maps of the Pilbara Craton are based on models constructed from often heavily weathered
326 samples of volcanic rock outcrops (Smith et al., 1982). The assessment of the metamorphic facies
327 in this study, however, is based on unweathered sedimentary rocks from drill cores. The difference
328 between the two data sets could be because: (1) the metamorphism is more spatially heterogeneous
329 than previously documented, or (2) studies of the metamorphism of highly weathered volcanic
330 rocks may result in difficulties in the correct evaluation of the metamorphic history, because the
331 presence or absence of metamorphic index minerals may be influenced by weathering. Regardless,
332 the current study of the metamorphism of the sedimentary rocks in the AIDP cores suggests
333 considerably more elevated temperatures than suggested previously (Smith et al., 1982). This
334 supports the organic geochemical data from French et al. (2015) who showed that polycyclic

aromatic hydrocarbons (PAHs) and diamondoids dominate these rocks, which are a characteristic of high thermal alteration, without indicating any particular temperature.

3.2. Assessment of carbonate veins and their enclosed organic matter

3.2.1 Petrography of carbonate veins

Although greenschist facies metamorphism has rendered the primary sedimentary rocks from cores AIDP-2 and AIDP-3 unsuitable for biomarker analysis, oil-bearing fluid inclusions and solid bitumen are present in two types of secondary carbonate veins. The carbonate composition of veins and their host matrix are shown in Figure 2. The vein carbonates of the Carawine Dolomite are similar to their host rock, but the vein carbonates of the Jeerinah Formation have different compositions relative to their host rock. Consequently, the carbonate veins of the Carawine Dolomite and the Jeerinah Formation are here defined as type 1 and type 2 veins, respectively (Fig. 2). The type 1 veins consist of subhedral dolomite, euhedral quartz and solid bitumen and contain oil-bearing fluid inclusions (Fig. 4A). The veins are relatively common between 180–260 m in AIDP-2 and appear as horizontal fracture fillings parallel to bedding, or as void fillings in some dolomite breccia. Metamorphosed wall rock fragments (mm-sized) are partly included in the vein matrices (Fig. 4A) indicating that greenschist-facies metamorphism pre-dates emplacement of the veins. Fuzzy dolomite boundaries of the veins (Fig. 4A) suggest that they are replacement veins, which means that they were formed by local alteration of the wall rock by incoming externally derived fluids along a fracture plane (Passchier and Trouw, 2005). Quartz is seen to be central in the veins, suggesting that a second stage of fluid influx was dominated by a Si-rich fluid. The undulose extinction (Fig. 4C) and the presence of subgrain boundaries in quartz (Fig. 4E) do not

356 necessitate high grade crystal-plastic deformation but can be attributed to growth related defects
357 when the crystals grow into an open space (e.g., Timms et al. 2009).
358

359

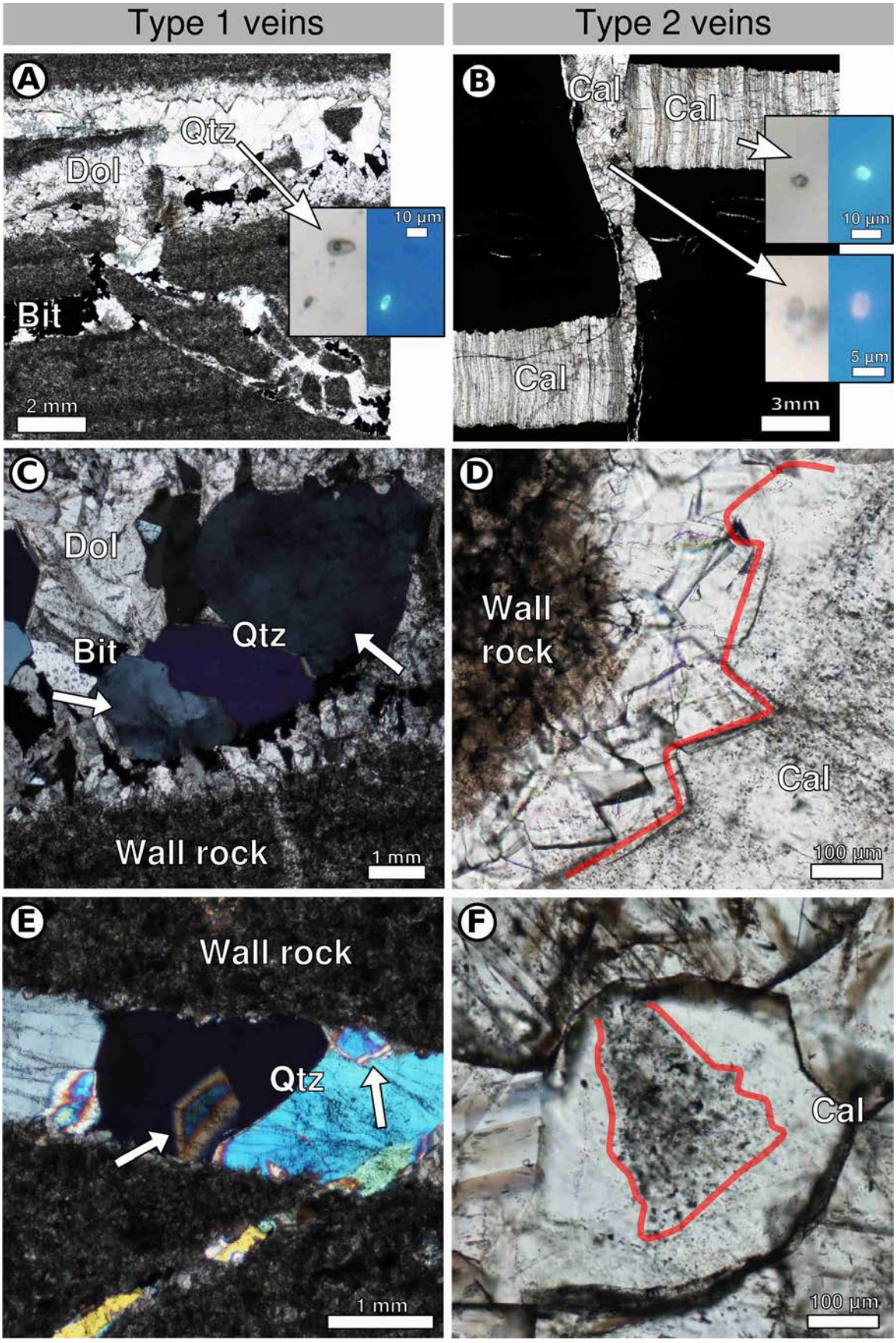
Type 1 veins
Type 2 veins
A
Qtz
Dol
Bit
10 µm
2 mm
B
Cal
Cal
Cal
10 µm
5 µm
3mm
C
Dol
Qtz
Bit
Wall rock
1 mm
D
Wall rock
Cal
100 µm
E
Wall rock
Qtz
1 mm
F
Cal
100 µm

Figure 4: Microstructures and oil-bearing fluid inclusions of the AIDP veins. Photomicrographs are of (A, C, E) type 1 veins of the Carawine Dolomite (AIDP-2/184.58m, S18), and (B, D, F) type 2 veins of the Jeerinah Formation (B, F: AIPD-3/162.69m, S77; D: AIDP-2/295.75m, S38) taken under plane polarisation (A, B, D, F) and crossed polarisation (C, E). Insets are photomicrographs of oil-bearing fluid inclusions shown under UV light (right) and plain light (left). Arrows in (C) point to undulose extinction, and in (E) to sub-grains. The wall rocks predominantly consist of a dolomitic matrix. Red lines in (D) and (F) indicate boundaries beyond which fluid inclusions have been removed by grain boundary migration (clear areas). The black dots are aqueous and oil-bearing fluid inclusions as well as closely associated μm-sized solid bitumen. Dol = dolomite, Qtz = quartz, Bit = solid bitumen, Cal = calcite.

The type 2 veins consist of either fibrous or blocky crystals of calcite and are restricted to the Jeerinah Formation. They appear between 290–310 m and 145–170 m in AIDP-2 and AIDP-3, respectively, and are more common in AIDP-3. Most lithotypes within the Jeerinah Formation have a meta-shale matrix, with dolomite, ankerite and siderite/ rhodochrosite as carbonate minerals, whereas the type 2 veins consist almost exclusively of calcite (Fig. 2). Veins with blocky crystals are thought to originate from fractures that fill quickly after opening where the growth location is central to the vein. In contrast, fibrous veins are typically formed by continuous opening and simultaneous growth of calcite (Bons et al., 2010). The Jeerinah Formation blocky and fibrous veins are mutually crosscutting, hence they must have formed contemporaneously. The blocky type 2 veins are rich in fluid inclusions and wall rock fragments giving the veins a cloudy, speckled appearance (Fig. 4D,F). The spatial relationship between cloudy and non-cloudy areas suggests that grain boundaries migrated across parts of a grain, sweeping up the impurities and fluid

inclusions and leaving clear areas of calcite behind, similar to features demonstrated in experiments by Schmatz and Urai (2011) (Fig. 4D,F). In contrast, there are no clear microstructural features that suggest significant grain boundary migration in fibrous calcite. The rate of migration of boundaries is significantly enhanced in the presence of fluids (e.g., Passchier and Trouw, 2005). Consequently, the migration of grain boundaries seen in the blocky veins but not in the fibrous veins may have been due to a higher content of water in the blocky grains and their grain boundaries due to rapid closure and fluid trapping. This is supported by the markedly higher abundance of fluid inclusions in the blocky veins. Accordingly, no temperature-driven grain boundary network modifications are observed in any type 2 veins. The type 2 veins contain µm-sized wall rock fluid inclusion bands (S-Fig. 2) especially in the blocky veins (Fig. 4B,D), which is consistent with rapid fracturing and healing for the blocky veins. The lack of metamorphic overprint for the type 2 veins but the observation that they include metamorphosed wall rock fragments, suggests that they must have formed after peak metamorphism, as was also the case for the type 1 veins.

3.2.2 Petrography of organic matter

Oil-bearing fluid inclusions occur in quartz crystals in type 1 veins and in calcite in type 2 veins (Fig. 4A,B). In the type 1 veins the oil-bearing fluid inclusions are colourless under transmitted light and some have black rims. Oil-bearing fluid inclusions are small, 1–8 µm in diameter, have round to irregular shapes, and contain ca. 10 vol% of a gas phase. It is difficult to determine whether they are primary or secondary fluid inclusions since they are so rare and isolated that no distribution patterns (e.g., overgrowths or fracture trails) are evident. They can be considered as primary within the veins as they were detected only in the quartz grains and not in the vein dolomite or rock matrices. However, it cannot be excluded that oil-bearing fluid inclusions are present in

406 the rock matrix as it is difficult to detect them visually in a dark, fine-grained rock matrix. Under
407 UV light they fluoresce mostly pale blue, but some have fluorescence colours varying from white
408 and yellow to orange. The intensity of the fluorescence is very low, which gives them a dim
409 appearance. In general, the black-rimmed oil-bearing fluid inclusions are dimmer than the others,
410 which may be attributed to an oil alteration effect caused by the degradation of aromatic
411 hydrocarbons (e.g., Radke, 1988). It is widely agreed that fluorescence of organic matter such as
412 macerals is intense in immature samples, but decreases during catagenesis and usually disappears
413 by the end of the oil window (Killops and Killops, 2009). Stasiuk and Snowdon (1997) have also
414 shown a similar process, with an intensity decrease in the fluorescence of more mature oil-bearing
415 fluid inclusions. The alteration of the oil-bearing fluid inclusions in the type 1 veins likely occurred
416 during minor recrystallisation of the type 1 veins. Grain boundary network modification by some
417 grain boundary migration is most likely the prominent cause of their alteration, as recrystallisation
418 processes have been shown to alter aqueous fluid inclusions (e.g., Schmatz and Urai, 2011). This
419 may likewise happen to fluid inclusions filled with oil. An alteration process may also explain the
420 black rims, as organic molecules were cracked to gas and only a bituminous material remained at
421 the rims, which appears black and slightly fluorescent under UV light. Other organic matter in the
422 type 1 veins is present as mm-sized blocks of solid bitumens (Fig. 4A). These are closely associated
423 with the quartz and are therefore likely to be syngenetic. The solid bitumens are black and non-
424 fluorescent under UV light, which indicates high thermal maturity (Curiale, 1986; George et al.,
425 1994). The precursor of the solid bitumens (probably free oil) may have been altered to a greater
426 extent than the quartz-hosted oil-bearing fluid inclusions, because the latter were protected by the
427 enclosing quartz (George et al., 2008).

The oil-bearing fluid inclusions in the type 2 veins are colourless under transmitted light and some have black rims. The oil-bearing fluid inclusions are 3–9 μm in diameter, somewhat larger than the inclusions in the type 1 veins. They have spherical to round shapes, and some also contain ca. 10 vol% gas, 5 vol% solid bitumens, and 5 vol% of an aqueous phase. Under UV light they fluoresce mostly pale blue, although some have yellow to orange fluorescence colours. The intensity of the fluorescence is very low, likely for the same reason as for type 1 veins. Movement of grain boundaries (Fig. 4D,F) could have redistributed and removed the oil-bearing fluid inclusions along with aqueous fluid inclusions, similar to experimental results of Schmatz and Urai (2011). Hence, only a few oil-bearing fluid inclusions were preserved in the calcite crystals, as others were moved and adsorbed onto the grain boundaries, likely as a thin layer of polar compounds (Fig. 4F) which can adsorb more readily to mineral surfaces (e.g., George et al., 2001). Because the process of migrating boundaries rearranged oil-bearing fluid inclusions along with aqueous fluid inclusions in the blocky calcite veins (Fig. 4D,F), they can be viewed as repositioned primary inclusions and thus not truly secondary inclusions. This interpretation is supported by oil-bearing fluid inclusions which were detected along growth zones seen the fibrous calcite veins. Hence, they are likely to be primary fluid inclusions incorporated during initial vein growth (Passchier and Trouw, 2005). Non-fluorescent solid bitumens occur between some of the oil-bearing-fluid inclusions in the calcite crystals and are μm-sized, unlike the mm-sized solid bitumens in the type 1 veins (Fig. 4D,F). Most likely these solid bitumens represent altered oil-bearing fluid inclusions.

3.2.3 Origin of the carbonate veins

On the basis of microstructural relationships, the oil-bearing fluid inclusions and solid bitumens in both vein types are probably the only features in which biomarkers can be expected to be found

in the AIDP cores. As described above, the veins were likely recrystallised, but to a lesser extent than the metasedimentary rocks. Calcite twinning geothermometry after Ferrill et al. (2004) was performed and homogenisation temperatures of aqueous fluid inclusions were derived to estimate the temperature that the veins experienced.

Only type 2 veins have been analysed using twinning geothermometry, as it applies only to calcite that has not experienced dynamic recrystallisation. Only thin twins, so called "type I" twins, were observed, indicating vein deformation under relatively low temperatures (Ferrill et al., 2004), which is in agreement with a crossplot of mean twin intensity versus mean twin width placing type 2 veins in a temperature field between 170 and 200°C (Fig. 5A, B). Homogenisation temperatures of aqueous fluid inclusions, which estimate the minimum temperature at which fluid inclusions were trapped inside the mineral grain (Goldstein and Reynolds, 1994), were assessed. Type 2 veins have homogenisation temperatures between 149–210°C, which corroborates the relatively mild formation temperatures calculated by the calcite twinning geothermometry method (Fig. 5). Ice-melting temperatures of the aqueous fluid inclusions range from -6.7 to -3.3°C (Fig. 5C). Based on eutectic temperatures of about -20°C, the H_2O–NaCl system (Goldstein and Reynolds, 1994) was used to calculate salinities for the type 2 vein fluid inclusions. Resulting salinities range from 5.4 to 10.1 wt% $NaCl_{equivalent}$. Type 1 veins have slightly higher homogenisation temperatures, ranging from 161–250°C. Fluid inclusions may stretch or leak during continued burial and during heating experiments, which results in homogenisation temperatures that are higher than recorded during the initial fluid entrapment (Goldstein and Reynolds, 1994). This is evident in the fluid inclusions in the type 1 veins, in which homogenisation temperatures occur over a wide range compared to homogenisation temperatures of fluid inclusions in the type 2 veins (Fig. 5C).

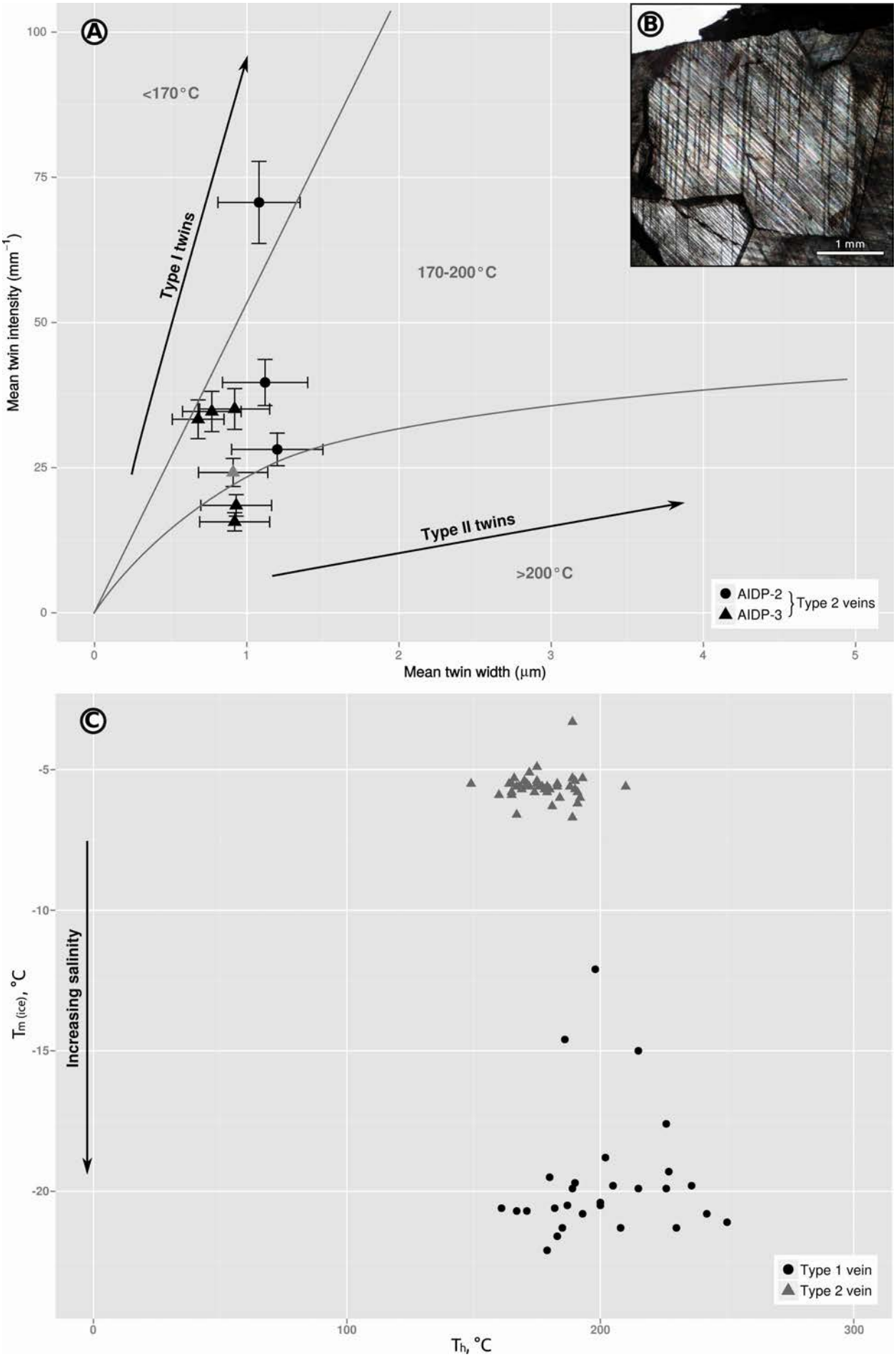
A
<170°C
Type I twins
170-200°C
Type II twins
>200°C
Mean twin intensity (mm⁻¹)
Mean twin width (μm)
AIDP-2
AIDP-3
Type 2 veins
B
1 mm
C
Increasing salinity
Tm (ice), °C
Th, °C
Type 1 vein
Type 2 vein

Figure 5: Carbonate vein geothermometry. (A) Calcite twinning geothermometry after Ferrill et al. (2004) of type 2 veins (calcite) of the Jeerinah Formation. Lines separate deformation temperatures, and arrows illustrate the paths of increasing strain as characterised by Ferrill et al. (2004). A systematic error of 10% is given. (B) Photomicrograph of sample AIDP-3/164.04 m (S87, Jeerinah Formation; plane polarisation) showing type I thin twins (for classification see Ferrill et al., 2004); this sample is indicated by the grey triangle in (A). (C) Homogenisation temperature (T_h) versus ice melting temperature ($T_{m,ice}$) for aqueous fluid inclusions from growth bands in carbonate crystals of samples S18 and S20 (type 1 veins) and samples S38 and S78 (type 2 veins). Eutectic temperatures were different in both veins, therefore resulting in two different systems for calculating salinities from ice melting temperatures (see text for details).

Generally the Ice-melting temperatures range from -22.1 to -12.1°C (Fig. 5C). The H_2O–NaCl–$CaCl_2$ system (Goldstein and Reynolds, 1994) was used to calculate salinities for the type 1 vein fluid inclusions, based on eutectic temperatures ranging between -66 and -70°C. Salinity estimates range from 16.0 to 23.1 wt% $NaCl_{equivalent}$, consistent with a hypersaline brine composition. To summarise, the two types of veins were not only formed after peak-metamorphism, but also under relatively mild temperature conditions from two different fluids, as shown by the calcite twinning and fluid inclusion homogenisation and ice-melting temperatures. Salinity increases with decreasing ice-melting temperatures (Goldstein and Reynolds, 1994).

Stable isotopes of the carbonates in the Carawine Dolomite range from ca. -4 to -13‰ in $\delta^{18}O_{VPDB}$ and +1 to -7‰ in $\delta^{13}C_{VPDB}$ (Fig. 6) and are consistent with the distribution pattern of the Carawine

Dolomite previously described by Veizer et al. (1989). Notably, the veins are more depleted in ^{18}O than the sedimentary dolomites, a process explained by dissolution and reprecipitation during the burial history (e.g., Veizer et al., 1989). Dissolved and reprecipitated surrounding sedimentary dolomites inside the vein would also explain the general chemical similarity of the carbonates in the Carawine Dolomite (Fig. 2) and why no oil-bearing fluid inclusions have been found in the vein dolomite, because sedimentary dolomites are depleted of them. Shale (PAAS; Taylor and McLennan, 1985) normalised REE+Y patterns of sedimentary dolomite of the Carawine Dolomite are light REE (LREE) depleted, have positive La and Eu anomalies, a superchondritic Y/Ho ratio and lack a Ce anomaly (S-Fig. 3, S-Table 2), consistent with previously documented late Archean marine carbonates (e.g., Bolhar et al., 2004; Kamber et al., 2014). Associated type 1 vein dolomite has very similar patterns with higher REE concentrations but no La anomaly, a very minor negative Ce anomaly and a very subdued Eu anomaly. Hence, the REEs were probably derived mostly from dissolution of local dolomite. The precursor fluids of type 1 veins may have been an organic-silica-rich acidic fluid, as shown by the mineral composition and the dissolution of the surrounding rocks.

Stable isotopes of the sedimentary carbonates in the Jeerinah Formation range from -1 to -15‰ in $\delta^{13}C_{VPDB}$ and -8 to -13‰ in $\delta^{18}O_{VPDB}$. In contrast, the type 2 veins range from -4 to -18‰ in $\delta^{13}C_{VPDB}$ and -12 to -18‰ in $\delta^{18}O_{VPDB}$ (Fig. 6), and likely originated from a hydrothermal system (e.g., Hecht et al., 1999). Thus, type 2 carbonate veins are chemically different in terms of major elements from the sedimentary carbonate of the Jeerinah Formation (Fig. 2), but they are isotopically similar, with the veins being on average slightly more depleted in ^{18}O (Fig. 6).

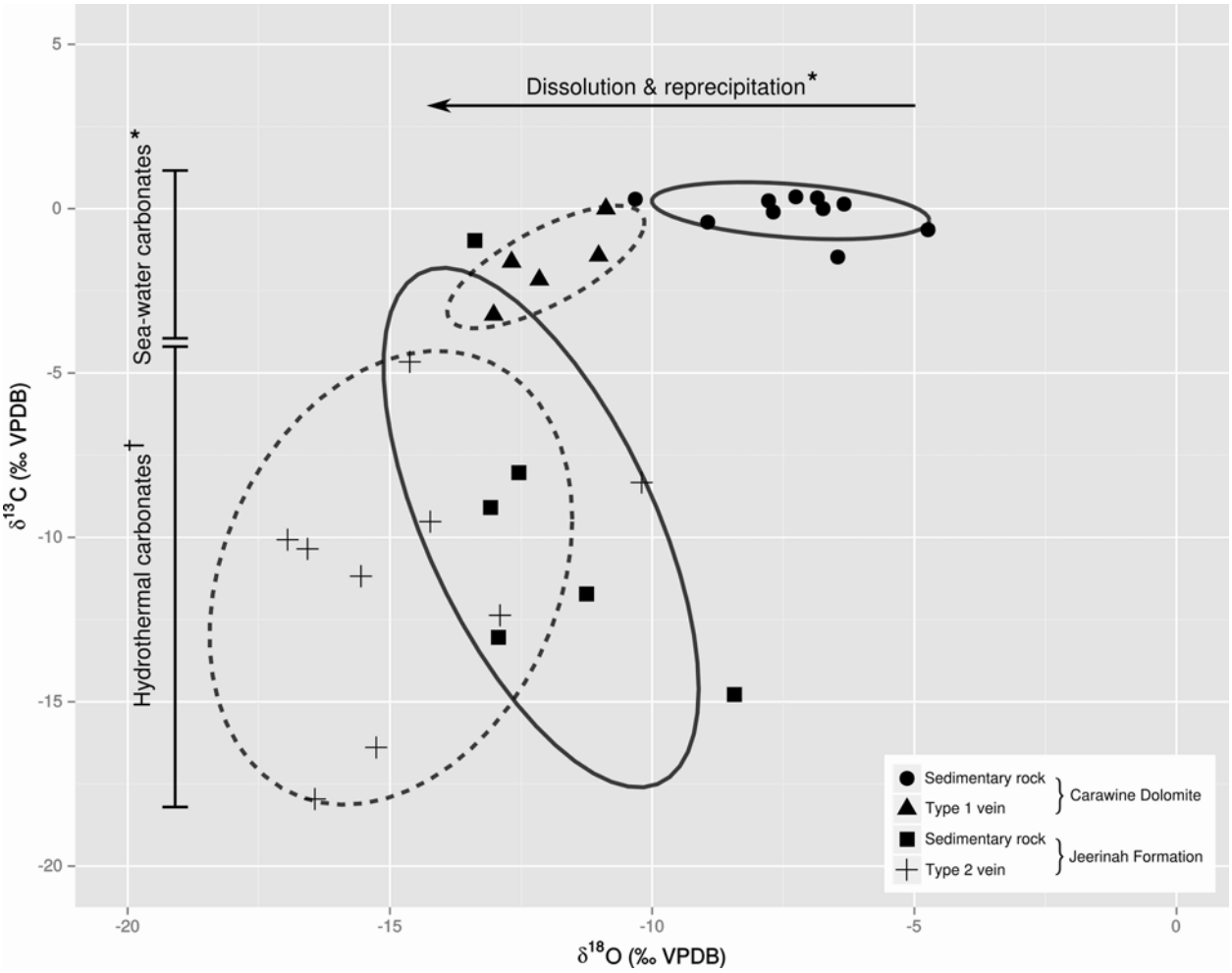

Figure 6: Scatter diagram of $\delta^{18}O$ versus $\delta^{13}C$ values for carbonates from the Jeerinah Formation and the Carawine Dolomite. Ellipses indicate an 85% area of confidence. † after Hecht et al. (1999), * after Veizer et al., (1989), based on typical values.

The type 2 veins are enriched in REEs relative to PAAS, and PAAS-normalised REE+Y patterns are enriched in the middle range and have a positive Eu anomaly (S-Fig. 3, S-Table 3). This REE+Y signature is consistent with the signature of hydrothermal carbonates (Hecht et al., 1999; Barrat et al., 2000) and the stable isotopes. The normalised REE+Y signature of type 2 carbonate veins further shows that both the blocky and the fibrous veins are closely connected, wherein the

528 blocky veins may have served as feeding channels for the fluid from which the fibrous veins
529 precipitated. The fibrous calcites are slightly LREE depleted (S-Fig. 3) consistent with water-rock
530 interaction between a hydrothermal fluid and the shale, possibly under slightly acidic conditions
531 (Hecht et al., 1999). It was not possible to analyse REE+Y in sedimentary dolomites within the
532 shales as they are too rare and intensely intergrown within the rock matrix. However, a likely
533 oceanic hydrothermal fluid as a precursor for the type 2 veins would agree with the relatively low
534 salinities of aqueous fluid inclusions, which are ca. 5–10 wt% $NaCl_{equivalent}$ (6–14 wt%
535 $NaCl_{equivalent}$; de Ronde et al., 1997).

536 **3.2.4 Age of the carbonate veins**

537 Attempts were made to date the two vein types. However, radiometric U-Pb or Pb-Pb dating using
538 LAM-ICP-MS was not successful due to the absence of mineral phases with sufficient radiogenic
539 U and Pb. Also, there was insufficient carbonaceous material for Re-Os dating.

540 Nevertheless, it is reasoned that the veins formed in the period between 2.2 and 1.8 Ga,
541 which represent the times of peak-metamorphism and the most recent regional uplift phase,
542 respectively (Dawson et al., 2002; Schmidt and Clark, 1994). Peak-metamorphism at 2.2
543 Ga is most likely the upper age limit of vein formation, as the veins crosscut the peak
544 metamorphic rocks and show significantly lower temperature estimates than the
545 surrounding rocks. In addition, both veins types contain metamorphosed wall rock
546 fragments. However, the lower age limit is more difficult to constrain. As the veins do not
547 show any meteoric oxygen isotope signature they cannot be unequivocally linked to the
548 uplift history of the area. During uplift, fluid circulation may involve non-meteoric fluids.
549 As both vein types are formed in the same temperature range, but carry different fluids as

shown by their chemical signature, they are likely to be related to a regional rather than local event. Hence the last known period of regional uplift marks the lower age limit of vein formation. The last uplift of the Mount Bruce Supergroup is recorded at 2.0 Ga and at 1.8 Ga in the lower Wyloo Group and upper Wyloo Group, respectively (e.g., Schmidt and Clark, 1994). Accordingly, the veins were most likely emplaced prior to 1.8 Ga.

Hence, we suggest that, albeit with significant uncertainty, the veins are Paleoproterozoic in age. Unfortunately, because of our relatively rudimentary knowledge of the fluid circulation history of the area, it is impossible to determine which formation(s) sourced the fluids from which the veins formed.

3.3 Pitfalls and opportunities for future biomarker studies

It is important to assess the organic geochemistry of the oil-bearing fluid inclusions and solid bitumens considering their possible Paleoproterozoic age in the present samples. When using bulk extraction of unoxidised rock samples, the presence of unconstrained (micro-)veins can easily be overlooked. Hence, biomarkers that originate from the veins may be mistaken for being indigenous to a sedimentary rock, when they actually originate from later veins, thus leading to incorrect interpretations. However, the presence of such veins in Precambrian rocks also provides a new opportunity to analyse very old biomarkers, particularly when the veins can be dated, and where metamorphism has destroyed any original biomarkers in the older host sedimentary rock. Nevertheless, it needs to be noted that the age of the formation from which the vein fluid originated may not always be easy to constrain unless the area has a long history of no tectonic or major hydrothermal modifications.

572 Attempts to analyse biomarkers in the organic matter captured in the veins presented here
573 were difficult. The analysis of oil-bearing fluid inclusions using established gas
574 chromatography-mass spectrometry (GC-MS) on-line or off-line methods (George et al.,
575 2012) was considered to be unsuitable due to the low frequency of occurrence of fluid
576 inclusions. Any GC-MS signal of the few oil-bearing fluid inclusions would be below the
577 blank levels. Other technical possibilities for analysis of the detected oil-bearing fluid
578 inclusions and/or solid bitumens include laser micropyrolysis GC-MS (e.g., Greenwood et
579 al., 1998) or Time of Flight-Secondary Ion Mass Spectrometry (ToF-SIMS; e.g., Siljeström
580 et al., 2010). The problem with applying ToF-SIMS to oil-bearing fluid inclusions is the
581 inclusions size, as current ToF-SIMS instruments are only able to analyse fluid inclusions
582 measuring about 15 μm (Siljeström et al., 2010), but the oil-bearing fluid inclusions
583 detected here are all < 8 μm. Laser micropyrolysis GC-MS seems to be more suitable
584 considering the fluid inclusion size, but only low to medium molecular weight
585 hydrocarbons can usually be detected (no hopanes or steranes; e.g., Greenwood et al.,
586 1998). The carbonate matrix of most veins is another problem, as other non-defined
587 hydrocarbons could be included (e.g., Nabbefeld et al., 2010). However, there are a few
588 possibilities for obtaining organic geochemical data, for example by using ToF-SIMS on
589 the solid bitumens, or by carrying out bulk solvent extraction of the veins with the
590 deduction of partial analysis of oil-bearing fluid inclusions and solid bitumens. The latter
591 technique applied to the AIDP veins will be the subject of a separate paper.

592 This discussion demonstrates not only the difficulties in obtaining reliable biomarker data
593 for a set of high thermal maturity metamorphosed sedimentary rocks, but also the
594 opportunities if unmetamorphosed organic material is contained in veins that post-date

595 regional metamorphism. This work shows the necessity for a major area of technique
596 development in organic geochemistry allowing analysis of increasingly smaller amounts
597 of organic material. The ability to obtain biomarkers from limited amounts of pristine
598 Archean rocks, such as from drill-cores, is essential for the investigation of signatures of
599 early life on Earth. These techniques would also be applicable to the analysis of extremely
600 expensive samples from sample-return missions to moons or planets such as Mars, where
601 sample size will be very limited.

602 **4 CONCLUSIONS**

603 Oil-bearing fluid inclusions and solid bitumens are preserved in two distinct types of carbonate
604 veins in the AIDP-2 and AIDP-3 cores from the Pilbara Craton. The Archean host rocks have been
605 metamorphosed to the greenschist facies and have experienced temperatures in excess of 300°C
606 and probably ~ 400°C, much higher than previously assumed. This explains the non-detection of
607 biomarkers in the fine-grained lithologies from the Pilbara Craton in earlier studies (French et al.,
608 2015). The first vein type occurs in the ca. 2.55 Ga Carawine Dolomite, and consists of quartz and
609 solid bitumen formed from an organic-silica-rich acidic fluid and reprecipitated dolomite. The
610 second vein type occurs in the ca. 2.65 Ga Jeerinah Formation, and includes calcite veins with a
611 hydrothermal source. Both vein types formed below 200°C and postdate regional greenschist
612 facies metamorphism, which has rendered them favourable for the potential preservation of
613 biomarkers. Unfortunately it was not possible to date the veins, but on the basis of known regional
614 metamorphic and tectonic events we propose a Paleoproterozoic age, albeit with significant
615 uncertainty. Recent advances in radiometric dating, combined with biomarker studies on oil-
616 bearing fluid inclusions and solid bitumens in veins, open new opportunities in the search for the

evidence of early life. Furthermore, such veins are not restricted to the least metamorphosed Archean sedimentary rocks, which are to be found in the Pilbara, Kaapvaal and Superior cratons.

This study emphasises the importance of careful petrological assessment of not only Archean rock samples, but also other Precambrian and organic-lean rock samples, in order to make accurate interpretations of biomarker data. For instance, without close petrographic assessment of the rocks it would be easy to inadvertently extract a (micro-)vein, which could be much younger, and might yield organic material that is not representative of the host rock. This close connection between petrology and organic geochemistry is crucial for future studies that seek to detect and reconstruct the early biosphere and the onset of oxygenic photosynthesis on Earth.

ACKNOWLEDGMENTS

We thank D. Birch and N. Vella from the Microscopy Unit, Faculty of Science and Engineering, Macquarie University, for help and technical assistance with microscopy. M. Bebbington is thanked for preparing the polished sections and S. Craven is thanked for help with the SelFrag. We thank D. Adams and W. Powell for help and technical assistance with major, minor, and trace element analysis. J. Cali from RSES at the Australian National University is thanked for the help and assistance with the isotopic data, and The Society for Organic Petrology (TSOP) is thanked for its funding with a Spackman Award awarded to C.A.P. We acknowledge J. Schmatz (University of Aachen, Germany) for discussion regarding the vein microstructures. We thank three anonymous reviewers for valuable comments that improved this work. Macquarie University is thanked for a PhD scholarship awarded to C.A.P. We gratefully thank the Agouron Institute for funding the AIDP drilling and sample analyses, and the Australian Research Council (DP130102547) for funding.

639 **REFERENCES**

640 Anbar, A. D., Duan, Y., Lyons, T. W., Arnold, G. L., Kendall, B., Creaser, R. A., Kaufman, A.
641 J.,Gordon, G. W., Scott, C., Garvin, J., Buick, R., 2007. A whiff of oxygen before the great
642 oxidation event? Science 317 (5846), 1903–1906. doi:10.1126/science.1140325

643 Barrat, J. A., Boulegue, J., Tiercelin, J. J., Lesourd, M., 2000. Strontium isotopes and rare-earth
644 element geochemistry of hydrothermal carbonate deposits from Lake Tanganyika, East
645 Africa. Geochimica et Cosmochimica Acta 64 (2), 287–298. doi:10.1016/S0016-
646 7037(99)00294-X

647 Bolhar, R., Kamber, B. S., Moorbath, S., Fedo, C. M., Whitehouse, M. J., 2004. Characterisation
648 of early Archaean chemical sediments by trace element signatures. Earth and Planetary
649 Science Letters 222 (1), 43–60. doi:10.1016/j.epsl.2004.02.016

650 Bons, P. D., Elburg, M. A., Gomez-Rivas, E., 2012. A review of the formation of tectonic veins
651 and their microstructures. Journal of Structural Geology 43, 33-62.
652 doi:10.1016/j.jsg.2012.07.005

653 Brasier, M. D., Antcliffe, J., Saunders, M., Wacey, D., 2015. Changing the picture of Earth's
654 earliest fossils (3.5–1.9 Ga) with new approaches and new discoveries. Proceedings of the
655 National Academy of Sciences, 112(16), 4859-4864. doi:10.1073/pnas.1405338111

656 Brocks, J. J., 2011. Millimeter-scale concentration gradients of hydrocarbons in Archean shales:
657 Live-oil escape or fingerprint of contamination? Geochimica et Cosmochimica Acta 75 (11),
658 3196–3213. doi:10.1016/j.gca.2011.03.014

659 Brocks, J. J., Buick, R., Logan, G. A., Summons, R. E., 2003. Composition and syngeneity of
660 molecular fossils from the 2.78 to 2.45 billion-year-old Mount Bruce Supergroup, Pilbara

Craton, Western Australia. Geochimica et Cosmochimica Acta 67 (22), 4289–4319. doi:10.1016/S0016-7037(03)00208-4

Brocks, J. J., Logan, G. A., Buick, R., Summons, R. E., 1999. Archean molecular fossils and the early rise of eukaryotes. Science 285 (5430), 1033–1036. doi:10.1126/science.285.5430.1033

Bucher, K., Grapes, R., 2011. Petrogenesis of Metamorphic Rocks, 8th Edition. Springer, 1–428. doi:10.1007/978-3-540-74169-5

Curiale, J. A., 1986. Origin of solid bitumens, with emphasis on biological marker results. Organic Geochemistry 10 (1-3), 559–580. doi:10.1016/0146-6380(86)90054-9

Dawson, G. C., Krapež, B., Fletcher, I. R., McNaughton, N. J., Rasmussen, B., 2002. Did late Palaeoproterozoic assembly of proto-Australia involve collision between the Pilbara, Yilgarn and Gawler cratons? Geochronological evidence from the Mount Barren Group in the Albany–Fraser Orogen of Western Australia. Precambrian Research 118 (3), 195–220. doi:10.1016/S0301-9268(02)00110-9

De Ronde, C. E. J., deR Channer, D. M., Faure, K., Bray, C. J., Spooner, E. T. C., 1997. Fluid chemistry Archean seafloor hydrothermal vents: implications for the composition of circa 3.2 Ga seawater. Geochimica et Cosmochimica Acta 61 (19), 4025–4042. doi:10.1016/S0016-7037(97)00205-6

Dutkiewicz, A., Volk, H., George, S. C., Ridley, J., Buick, R., 2006. Biomarkers from Huronian oil-bearing fluid inclusions: An uncontaminated record of life before the Great Oxidation Event. Geology 34 (6), 437–440. doi:10.1130/G22360.1

Dutkiewicz, A., Rasmussen, B., Buick, R., 1998. Oil preserved in fluid inclusions in Archaean sandstones. Nature 395 (6705), 885–888. doi:10.1038/27644

683 Eigenbrode, J. L., Freeman, K. H., Summons, R. E., 2008. Methylhopane biomarker hydrocarbons
684 in Hamersley Province sediments provide evidence for Neoarchean aerobiosis. Earth and
685 Planetary Science Letters 273 (3), 323–331. doi:10.1016/j.epsl.2008.06.037
686 Ferrill, D. A., Morris, A. P., Evans, M. A., Burkhard, M., Groshong Jr, R. H., Onasch, C. M., 2004.
687 Calcite twin morphology: a low-temperature deformation geothermometer. Journal of
688 Structural Geology 26 (8), 1521–1529. doi:10.1016/j.jsg.2003.11.028
689 French, K. L., Hallmann, C., Hope, J. M., Schoon, P. L., Zumberge, J. A., Hoshino, Y., Peters, C.
690 A., George, S. C., Love, G. D., Brocks, J. J., Buick, R., Summons, R. E., 2015. Reappraisal
691 of hydrocarbon biomarkers in Archean rocks. Proceedings of the National Academy of
692 Sciences 112 (19), 5915–5920. doi:10.1073/pnas.1419563112
693 George, S. C., Volk, H., Dutkiewicz, A., 2012. Mass spectrometry techniques for analysis of oil
694 and gas trapped in fluid inclusions. In: Lee, M. S. (Ed.), Mass Spectrometry Handbook. John
695 Wiley & Sons, Inc., 647–673. doi:10.1002/9781118180730.ch30
696 George, S. C., Volk, H., Dutkiewicz, A., Ridley, J., Buick, R., 2008. Preservation of hydrocarbons
697 and biomarkers in oil trapped inside fluid inclusions for> 2 billion years. Geochimica et
698 Cosmochimica Acta 72 (3), 844–870. doi:10.1016/j.gca.2007.11.021
699 George, S. C., Ruble, T. E., Dutkiewicz, A., Eadington, P. J., 2001. Assessing the maturity of oil
700 trapped in fluid inclusions using molecular geochemistry data and visually-determined
701 fluorescence colours. Applied Geochemistry, 16 (4), 451–473. doi:10.1016/S0883-
702 2927(00)00051-2
703 George, S. C., Llorca, S. M., Hamilton, P. J., 1994. An integrated analytical approach for
704 determining the origin of solid bitumens in the McArthur Basin, northern Australia. Organic
705 Geochemistry 21 (3), 235–248. doi:10.1016/0146-6380(94)90187-2

706 Gharrabi, M., Velde, B., Sagon, J. P., 1998. The transformation of illite to muscovite in pelitic
707 rocks: Constraints from X-ray diffraction. Clays and Clay Minerals, 46 (1), 79–88.
708 doi:10.1346/CCMN.1998.0460109
709 Goldstein, R. H., Reynolds, T. J., 1994. Systematics of fluid inclusions in diagenetic minerals:
710 SEPM short course 31. Society for Sedimentary Geology, 1–199. doi:10.2110/scn.94.31
711 Greenwood, P. F., George, S. C., Hall, K., 1998. Applications of laser micropyrolysis–
712 gaschromatography–mass spectrometry. Organic Geochemistry 29 (5), 1075–1089.
713 doi:10.1016/S0146-6380(98)00101-6
714 Hecht, L., Freiberger, R., Gilg, H. A., Grundmann, G., Kostitsyn, Y. A., 1999. Rare earth element
715 and isotope (C, O, Sr) characteristics of hydrothermal carbonates: genetic implications for
716 dolomite-hosted talc mineralization at Göpfersgrün (Fichtelgebirge, Germany). Chemical
717 Geology 155 (1), 115–130. doi:10.1016/S0009-2541(98)00144-2
718 Hunt, J. M., 1996. Petroleum Geology and Geochemistry. Freeman, New York., 1–743.
719 doi:10.1017/S0016756800007755
720 Kamber, B. S., Webb, G. E., Gallagher, M., 2014. The rare earth element signal in Archaean
721 microbial carbonate: information on ocean redox and biogenicity. Journal of the Geological
722 Society 171 (6), 745–763. doi:10.1144/jgs2013-110
723 Killops, S. D., Killops, V. J., 2009. Introduction to Organic Geochemistry. John Wiley & Sons,
724 Inc., 1–394. doi:10.1016/0016-7037(94)90396-4
725 Lanari, P., Wagner, T., Vidal, O., 2014. A thermodynamic model for di-trioctahedral chlorite from
726 experimental and natural data in the system MgO–FeO–Al_2O_3–SiO_2–H_2O: Applications to P–
727 T sections and geothermometry. Contributions to Mineralogy and Petrology 167 (2), 1–19.
728 doi:10.1007/s00410-014-0968-8

729 Nabbefeld, B., Grice, K., Schimmelmann, A., Summons, R. E., Troitzsch, U., Twitchett, R. J.,
730 2010. A comparison of thermal maturity parameters between freely extracted hydrocarbons
731 (Bitumen I) and second extract (Bitumen II) from within the kerogen matrix of Permian and
732 Triassic sedimentary rocks. Organic Geochemistry 41 (2), 78–87.
733 doi:10.1016/j.orggeochem.2009.08.004
734 Passchier, C. W., Trouw, R. A. J., 2005. Microtectonics, 2nd Edition. Vol. 256. Springer, 1–366.
735 doi:10.1007/3-540-29359-0
736 Planavsky, N. J., Asael, D., Hofmann, A., Reinhard, C. T., Lalonde, S. V., Knudsen, A., Wang,
737 X., Ossa Ossa, F., Pecoits, E., Smith, A. J. B., Beukes, N. J., Bekker, A., Johnson, T. M.,
738 Konhauser, K. O., Lyons, T. W., Rouxel, O. J., 2014. Evidence for oxygenic photosynthesis
739 half a billion years before the Great Oxidation Event. Nature Geoscience 7 (4), 283–286.
740 doi:10.1038/ngeo2122
741 Radke, M., 1988. Application of aromatic compounds as maturity indicators in source rocks and
742 crude oils. Marine and Petroleum Geology 5 (3), 224–236. doi:10.1016/0264-8172(88)90003-
743 7
744 Rashby, S. E., Sessions, A. L., Summons, R. E., Newman, D. K., 2007. Biosynthesis of 2-
745 methylbacteriohopanepolyols by an anoxygenic phototroph. Proceedings of the National
746 Academy of Sciences 104 (38), 15099–15104. doi:10.1073/pnas.0704912104
747 Rasmussen, B., Fletcher, I. R., Brocks, J. J., Kilburn, M. R., 2008. Reassessing the first appearance
748 of eukaryotes and cyanobacteria. Nature, 455 (7216), 1101–1104. doi:10.1038/nature07381
749 Rasmussen, B., Fletcher, I. R., Sheppard, S., 2005. Isotopic dating of the migration of a low-grade
750 metamorphic front during orogenesis. Geology 33 (10), 773–776. doi:10.1130/G21666.1

751 Schirmer, A., Rude, M. A., Li, X., Popova, E., Del Cardayre, S. B., 2010. Microbial biosynthesis
752 of alkanes. Science 329 (5991), 559–562. doi:10.1126/science.1187936
753 Schmatz, J., Urai, J. L., 2011. The interaction of migrating grain boundaries and fluid inclusions
754 in naturally deformed quartz: A case study of a folded and partly recrystallized quartz vein
755 from the Hunsrück Slate, Germany. Journal of Structural Geology 33 (4), 468–480.
756 doi:10.1016/j.jsg.2010.12.010
757 Schmidt, P. W., Clark, D. A., 1994. Palaeomagnetism and magnetic anisotropy of Proterozoic
758 banded-iron formations and iron ores of the Hamersley Basin, Western Australia. Precambrian
759 Research 69 (1-4), 133–155. doi:10.1016/0301-9268(94)90083-3
760 Siljeström, S., Lausmaa, J., Sjövall, P., Broman, C., Thiel, V., Hode, T., 2010. Analysis of hopanes
761 and steranes in single oil-bearing fluid inclusions using time-of-flight secondary ion mass
762 spectrometry (ToF-SIMS). Geobiology 8 (1), 37–44. doi:10.1111/j.1472-4669.2009.00223.x
763 Simonson, B. M., Hassler, S., 1997. Revised correlations in the early Precambrian Hamersley
764 Basin based on a horizon of resedimented impact spherules. Australian Journal of Earth
765 Sciences 44 (1), 37–48. doi:10.1080/08120099708728292
766 Simonson, B. M., Schubel, K. A., Hassler, S. W., 1993. Carbonate sedimentology of the early
767 Precambrian Hamersley Group of western Australia. Precambrian Research 60 (1), 287–335.
768 doi:10.1016/0301-9268(93)90052-4
769 Smith, R. E., Perdrix, J. L., Parks, T. C., 1982. Burial metamorphism in the Hamersley Basin,
770 Western Australia. Journal of Petrology 23 (1), 75–102. doi:10.1093/petrology/23.1.75
771 Stasiuk, L. D., Snowdon, L. R., 1997. Fluorescence micro-spectrometry of synthetic and natural
772 hydrocarbon fluid inclusions: Crude oil chemistry, density and application to petroleum
773 migration. Applied Geochemistry 12 (3), 229–241. doi:10.1016/S0883-2927(96)00047-9

774 Stüeken, E. E., Buick, R., Guy, B. M., Koehler, M. C. 2015. Isotopic evidence for biological
775 nitrogen fixation by molybdenum-nitrogenase from 3.2 Gyr. Nature, 520 (7549), 666-669.
776 doi:10.1038/nature14180
777 Summons, R. E., Jahnke, L. L., Hope, J. M., Logan, G. A., 1999. 2-Methylhopanoids as biomarkers
778 for cyanobacterial oxygenic photosynthesis. Nature 400 (6744), 554–557. doi:10.1038/23005
779 Taylor, S. R., McLennan, S. M., 1985. The continental crust: Its composition and evolution.
780 Blackwell Scientific Pub., 1–312. doi:10.1002/gj.3350210116
781 Thorne, A., Trendall, A. F., 2001. Geology of the Fortescue Group, Pilbara Craton, Western
782 Australia. Vol. 144. Geological Survey of Western Australia, Department of Minerals and
783 Energy, 1–249. doi: n/a
784 Timms, N. E., Li, J., Reddy, S. M., 2009. Quantitative microstructural characterization of
785 natrojarosite scale formed during high-pressure acid leaching of lateritic nickel ore. American
786 Mineralogist 94 (8-9), 1111-1119. doi:10.2138/am.2009.3104
787 Tissot, B. P., Welte, D. H., 1984. Petroleum formation and occurrence. Springer, 1–699.
788 doi:10.1007/978-3-642-87813-8
789 Van Kranendonk, M. J., Hugh Smithies, R., Hickman, A. H., Champion, D. C., 2007. Review:
790 secular tectonic evolution of Archean continental crust: interplay between horizontal and
791 vertical processes in the formation of the Pilbara Craton, Australia. Terra Nova, 19(1), 1–38.
792 doi:10.1111/j.1365-3121.2006.00723.x
793 Veizer, J., Hoefs, J., Lowe, D. R., Thurston, P. C., 1989. Geochemistry of Precambrian carbonates:
794 II. Archean greenstone belts and Archean sea water. Geochimica et Cosmochimica Acta 53
795 (4), 859–871. doi:10.1016/0016-7037(89)90031-8

796 Volkman, J. K., 2005. Sterols and other triterpenoids: source specificity and evolution of
797 biosynthetic pathways. Organic Geochemistry 36 (2), 139–159.
798 doi:10.1016/j.orggeochem.2004.06.013
799 Waldbauer, J. R., Sherman, L. S., Sumner, D. Y., Summons, R. E., 2009. Late Archean molecular
800 fossils from the Transvaal Supergroup record the antiquity of microbial diversity and
801 aerobiosis. Precambrian Research 169 (1), 28–47. doi:10.1016/j.precamres.2008.10.011
802 Welander, P. V., Coleman, M. L., Sessions, A. L., Summons, R. E., Newman, D. K., 2010.
803 Identification of a methylase required for 2-methylhopanoid production and implications for
804 the interpretation of sedimentary hopanes. Proceedings of the National Academy of Sciences
805 107 (19), 8537–8542. doi:10.1073/pnas.0912949107